GLACIER CHANGE IN THE CARIBOO MOUNTAINS OF BRITISH COLUMBIA, CANADA (1946 – 2011)

by

Matthew J. Beedle

B.S., Montana State University, 2000
M.A., University of Colorado – Boulder, 2005

THESIS SUBMITTED IN PARTIAL FULFILLMENT OF
THE REQUIREMENTS FOR THE DEGREE OF
DOCTOR OF PHILOSOPHY
IN
NATURAL RESOURCES AND ENVIRONMENTAL STUDIES

UNIVERSITY OF NORTHERN BRITISH COLUMBIA

January 2014

Abstract

This thesis is a five-chapter investigation of glacier change in the Cariboo Mountains of British Columbia. In chapter one I discuss the importance of glaciers, introduce the glaciers of the Cariboo Mountains, and outline the objectives and structure of this thesis.

In chapter two I compare three methods to estimate annual glacier mass balance of a 9.5 km^2 mountain glacier for years 2009, 2010, and 2011. I find two geodetic methods, real-time kinematic GPS (global positioning system) and photogrammetry, to provide a valuable measure of glacier-wide annual mass balance that is complementary to the glaciological method.

In chapter three I reconstruct the terminus position of the same mountain glacier for the period 1959-2007 from a series of annual push moraines. Annual recession of this glacier, the longest record for a North American glacier, is controlled by air temperature during the ablation season and accumulation season precipitation during the previous decade. I demonstrate an immediate glacier terminus reaction to summer and annual mass balance and a delayed reaction to winter and annual balance.

In chapter four I calculate dimensional change for 33 representative glaciers in the Cariboo Mountains for the latter half of the twentieth century. I show the period 1952-1985, when nine glaciers advanced, to be one of little net change for Cariboo Mountains glaciers. After 1985, however, rates of recession and thinning increased substantially. Comparison with climatological records reveals this marked change is due to both increased ablation season temperature and decreased accumulation season precipitation.

I show glacier response to climate over this period to be highly variable and that relations between response and glacier morphometry are not consistent temporally.

In chapter five I conclude this thesis with the progress gained through my research, study limitations, and the knowledge gaps that remain. Finally, I make 10 recommendations that will address knowledge gaps, and improve understanding of glacier change.

Table of Contents

List of Tables

List of Figures

Acknowledgement

I wish to thank my supervisors, Brian Menounos and Roger Wheate. I will fondly remember long slogs in the field, marmot-eaten vehicles and resulting logistics, cold beverages stashed in alpine creeks, and informal steam-room advice. Thanks are also due to my additional committee members - Stephen Déry, Peter Jackson and Shawn Marshall - who helped particularly to reign in the scope of my research.

Many individuals volunteered significant time and effort during field campaigns at Castle Creek Glacier, without which the work in chapter two would not have been possible. I thank Dennis Straussfogel, Theo Mlynowski, Joe Shea, Rob Vogt, Teresa Brewis, Brian Menounos, Roger Wheate, Andy Clifton, Stephen Déry, Rob Sidjak, Laura Thomson, Maria Coryell-Martin, Shawn Marshall, Amy Klepetar, Sonja Ostertag and Nicole Schaffer for their assistance.

I thank Brian Luckman for his assistance with chapter three. I'm thankful for his willingness to share the Castle Creek Glacier push moraines with me.

The work in chapter four would not have been possible without hours of work by Caillin Smith and Tyler Sylvestre who scanned many hundreds of aerial photos. I also would like to thank Christina Tennant for help with Vr Photogrammetry software.

This thesis is a product of the Western Canadian Cryospheric Network (WC^2N), of which I feel privileged to have been a part. I also would like to thank the Pacific Institute for Climate Solutions (PICS), whose graduate fellowship helped me complete my PhD research and pursue science communication and outreach objectives that were beyond the scope of my thesis.

Thanks to Amy, Finlay and Liam for patience and support.

1. Introduction

The primary focus of this thesis is to refine methods and use them to address shortfalls in our understanding of glacier change. I employ field-based and remote sensing methods to measure glacier change of the Cariboo Mountains of British Columbia (BC), Canada. A secondary focus of this thesis is the changes in extent and volume of glaciers of the Cariboo Mountains since the 1950s, and on the climatic drivers of this change.

1.1. Importance of glaciers

Glaciers are fundamental components of Earth's climate and hydrologic systems. Accumulation season snowfall and ablation season ice melt represent the primary factors that drive annual changes in glacier mass. Long-term changes in glacier mass balance ultimately control glacier fluctuations at time scales of a decade or more. Climate variability affects accumulation and ablation and results in glacier change with impacts on numerous natural and human systems.

A majority of Earth's freshwater is held in the ice and snow of glaciers. Glacier change thus serves as a governor of freshwater flow volume, flow timing, temperature, and quality in glacierized watersheds (e.g., Moore et al., 2009). Glacier recession can have adverse effects on municipal, agricultural and industrial water supply (e.g., Barnett et al., 2005; Marshall et al., 2011). Loss of glacier meltwater in a watershed may also impact riverine ecosystems and salmon productivity (Dorava and Milner, 2000), and coastal ecosystems through alteration of dissolved organic matter in rivers (Hood et al., 2009). Melting glaciers may also be a prominent source of persistent organic pollutants,

whereby pollutants which accumulate in glaciers through snowfall, are subsequently released during ice melt, often in concentrated amounts (e.g., Bogdal et al., 2009).

As glaciers change they can alter global sea level, which falls as glaciers expand and rises when glaciers shrink. Much uncertainty remains regarding the quantity and rate of ongoing and projected 21st century sea level rise (e.g., Meier et al., 2007; Radić and Hock, 2011; Rignot et al., 2011; and Jacob et al., 2012). It is plausible that glacier wastage will raise the global ocean by about 0.4 m by the end of this century (Bahr et al., 2009). Higher sea level rise from changes in global ice volume cannot be ruled out, due to a lack of understanding of the dynamic response of the Greenland and Antarctic ice sheets to current and projected warming (e.g., Rignot et al., 2011).

Glacier loss may increase geomorphic hazards such as rock fall, rock avalanches, debris flows, debris avalanches, and debris slides (e.g., Moore et al., 2009). Glacier change can also lead to flooding events through glacier outburst floods (ice or moraine dammed lakes). While most events occur in remote locations, notable exceptions exist where these floods caused significant damage to infrastructure and killed thousands of people (e.g., Huggel et al., 2008).

Glaciers also represent an important natural resource for mountain communities given their tourist appeal. Visitors contribute to local economies through glacier sightseeing, dogsledding, and climbing adventures. Additionally, some ski resorts rely heavily on glaciers for operations, including British Columbia resorts such as Whistler Blackcomb in the southern Coast Mountains and the proposed Jumbo Glacier Resort in the Purcell Mountains. In the Alps expensive efforts have been made in attempts to artificially preserve glaciers on which the ski industry depends (Smiraglia et al., 2008).

Glaciers receive their nourishment and are depleted by meteorological phenomena, but glaciers also control their local climate (e.g., Barry, 2002). Their highly reflective surfaces reflect shortwave radiation resulting in cool temperatures locally, regionally, and, in the case of major ice sheets, even continentally. This cooling also influences local winds and general atmospheric circulation. Conversely loss of high-albedo glacier surfaces results in warming and possible changes in atmospheric circulation.

Glacier change constitutes an independent, natural response of local-to-global climate change, especially for remote high-elevation locations where few meteorological measurements are made. Recent work has reconstructed global and hemispheric temperature records for the past 400 years from records of glacier recession (Leclercq and Oerlemans, 2011). Additionally, imagery of receding glaciers is among the most poignant depictions of recent climate change, and arguably plays a central role in the motivation to act on global warming:

> "If the world does address the great challenge of global warming, it will be in part because of the way that glaciers serve as icons to make this challenge visible."
>
> (Orlove et al., 2008)

1.2. Glaciers and ice caps

This thesis focuses on changes of glaciers and ice caps (GIC), a term used here to refer to all glaciers excluding the Greenland and Antarctic ice sheets. GIC surface area comprises approximately 683,000 km^2 (Arendt et al., 2012), and total volume is estimated to represent a sea level rise equivalent (SLE) of 43 cm (Huss and Farinotti, 2012). Most GIC exist in western North America, Central Asia, and the Arctic islands of

Canada, Norway, and Russia (Zemp and van Woerden, 2008). The majority of the GIC in continental North America are found in Alaska and western Canada. At present the GIC of western Canada (south of 60°N) represents an area of 26,000 km^2, with most of the glacierized area located in the Saint Elias and Coast mountains of BC (Bolch et al., 2010).

Glaciers and how they change are measured via remote sensing methods or through direct measurements in the field (e.g., Cogley, 2005; Barry, 2006; Bamber and Rivera, 2007). Remote sensing of glaciers can be applied to measure extent, surface elevation, and surface velocity across large areas. Field measurements of extent, surface elevation, density, thickness, and velocity are made at limited points for a given glacier. Many of these field measurements are made with much greater precision than with remote sensing techniques. Remote sensing methods yield a comprehensive picture of global GIC change since the 1980s; however, detailed field measurements of seasonal and annual GIC change are scarce, with much understanding of glacier change coming from a subset of some 30 global 'benchmark' glaciers (Zemp et al., 2009).

Remote sensing and field-based measurements have yielded a general understanding of global GIC mass loss. In many regions this loss has accelerated in recent decades, primarily driven by increased surface air temperatures (e.g., Kaser et al., 2006). There have been and continue to be some exceptions to this general pattern, however. Regionally, some GICs of New Zealand and Norway advanced during the 1990s (e.g., Zemp and van Woerden, 2008), and GICs of the western Karakoram were noted to be growing in the 1990s (Hewitt, 2005); more recent work indicates that these latter glaciers are gaining mass (Gardelle et al., 2012). In each of these regions, gains in

mass and glacier advance have been attributed to increased accumulation-season snowfall, but also to complex high-elevation topography and the role of debris cover in the case of Karakoram GIC. Other individual glaciers that are an exception to the general pattern of recession have unique, marine-terminating ice dynamics (e.g., Ritchie et al., 2008; Truffer et al., 2009). However, the dominant global pattern is of GIC mass loss and recession, and is projected to continue throughout the 21st century and contribute significantly to global sea level (e.g., Radić and Hock, 2011).

1.3. Glaciers of the Cariboo Mountains

This thesis examines glaciers and glacier change of the Cariboo Mountains in the central interior of BC (Fig. 1.1). These glaciers, at the northern extent of the Columbia Mountains, are at the headwaters of the Fraser, North Thompson (a tributary of the Fraser) and Columbia rivers. The 200-km long Cariboo Mountains are bounded by the Rocky Mountain Trench and Rocky Mountains to the north and east respectively, the North Thompson River valley and Selkirk Mountains to the south, and the Interior Plateau to the west (Figure 1.1). Bowron Lake, Cariboo Mountains, and Wells Gray Provincial Parks lie at the western edge of the range.

The climate of the Cariboo Mountains is influenced by maritime and continental air masses, but the annual precipitation of the western margins of the range is high, with mean annual precipitation of 788-1,240 mm. This interior temperate rainforest, or wetbelt, is characterized by much higher precipitation than in the surrounding regions (Stevenson et al., 2011).

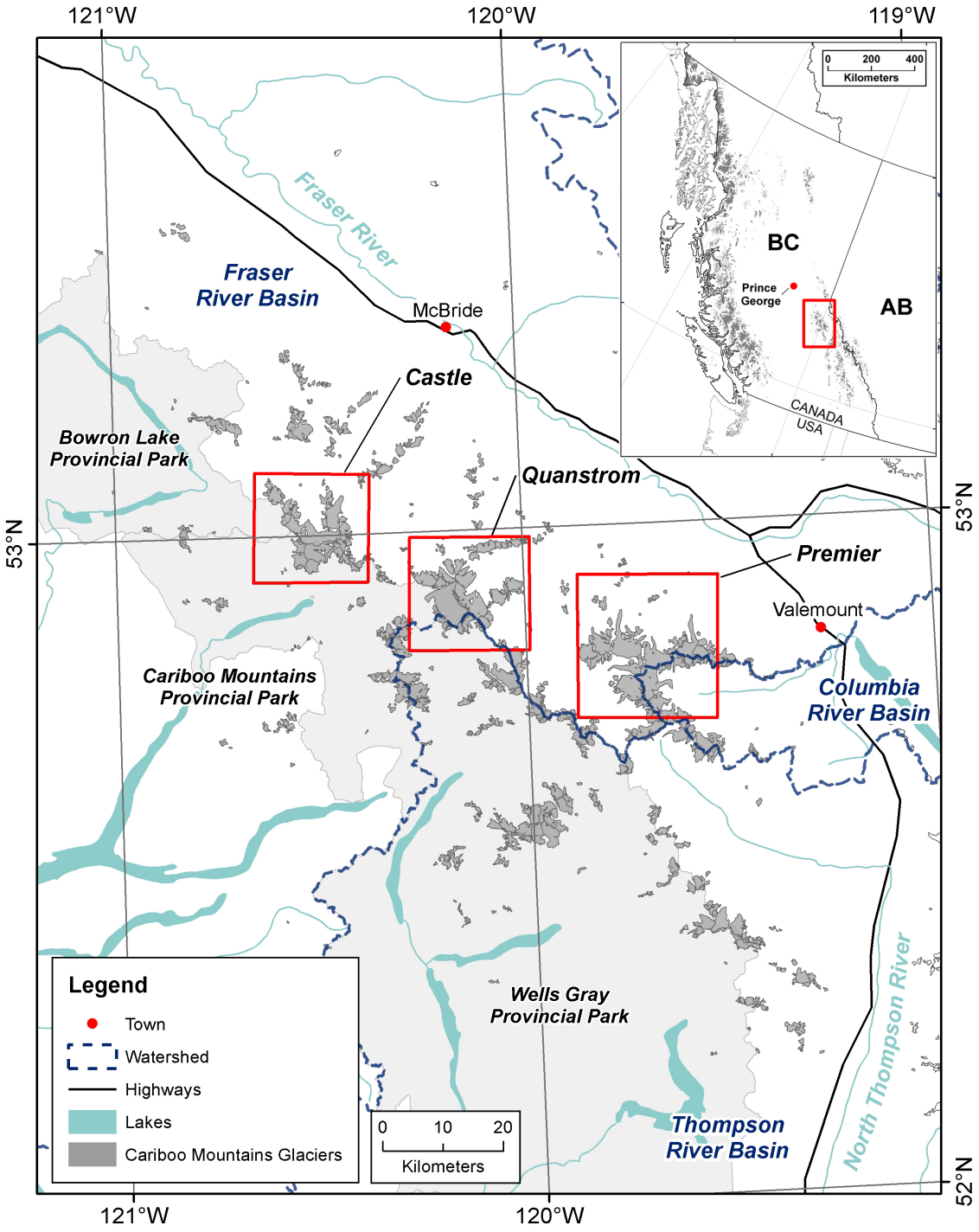

Figure 1.1 Study area. The three red rectangles indicate subregions of focus in this thesis (Castle, Quanstrom, and Premier). All western Canada glaciers, below 60°N (Bolch et al., 2010) are shown in the inset in gray, along with the location of the Cariboo Mountains (red rectangle).

Bolch et al. (2010) completed the first comprehensive inventory of the glaciers of western Canada. This data set includes the 526 glaciers of the Cariboo Mountains, which shrank from 845 km^2 in 1985 to 731 km^2 in 2005, a loss of 114 km^2 or 13%. Schiefer et al. (2007) derived volume change of all BC glaciers for the period 1985-1999. This data set indicates Cariboo Glaciers lost -0.47 km^3 a^{-1} for this period, equivalent to a thinning rate of -0.58 m a^{-1} (both values expressed in units of water equivalent). In the earliest previous study to focus explicitly on glaciers of the Cariboo Mountains, Luckman et al. (1986) studied 31 termini of glaciers in the Premier Range of the southern Cariboo Mountains. They found most of these glaciers advanced during the 1970s, and they attributed this advance to: (1) increased winter precipitation during the period 1951-1976; and (2) cooler than average summer temperatures from the period 1954-1968. Brewis (2012) examined glacier change in the Canoe Basin (a subset of Premier Range glaciers) and found glaciers shrank and lost volume from 1948-2005, but that their recession slowed and some advanced during the period 1955-1985.

1.4. Thesis objectives and outline

Previous work has synthesized the current understanding of global glacier change and made recommendations for future efforts and areas of focus (e.g., Fountain et al., 1999; Haeberli et al, 2007; Paul et al., 2007; Zemp et al., 2009). These studies recommend: (1) validating and calibrating field measurements with repeat mapping of glacier surface elevation; (2) extending annually measured glaciers to remote regions that are underrepresented; and (3) detailing strategies to study regional-to-global glacier change through a tiered approach. The two primary objectives of this thesis are built

upon these recommendations. The first objective of this thesis is to develop and test new methods that address glacier change. The second objective of this thesis is to determine glacier change of the Cariboo Mountains since the 1950s and the climatic drivers of this change.

This thesis is paper-based, and chapters 2, 3, and 4 are written as stand alone papers. I have made slight modifications to chapter content in this thesis to reduce repetition; these modifications are restricted to the introductory content of each chapter. At the beginning of each chapter I note the status of each paper within the peer-review process, which varies by chapter from 'published' to 'in preparation'.

In chapter two, I compare glaciological, photogrammetric and real-time kinematic global positioning system (RTK GPS) methods of measuring annual mass balance of Castle Creek Glacier within the Castle region of the Cariboo Mountains. This chapter illustrates the facility of geodetic methods to improve our understanding of glacier mass balance, and recommends best practices for future mass-balance studies. This chapter is 'in press' in Journal of Glaciology (Beedle et al., *in press*).

Chapter three documents a series of annual push moraines in the forefield of Castle Creek Glacier. From these geomorphic features I reconstruct the longest annually-resolved record of glacier length change for a North American glacier (1959-2007), and relate these changes to regional climate variability. This chapter has been peer reviewed and is published in Geophysical Research Letters (Beedle et al., 2009).

In chapter four, I use aerial photogrammetry to investigate the extent and volume change of Cariboo Mountains glaciers from the 1950s to 2005. This chapter focuses on a subset of glaciers from three subregions of the Cariboo Mountains. From northwest to

southeast these are the Castle, Quanstrom, and Premier regions, which include most of the glaciers in the Cariboo Mountains (Fig. 1.1). This chapter has not been peer reviewed and is in preparation for submission to The Cryosphere (Beedle et al., *in prep.*).

I conclude this thesis with a fifth chapter that synthesizes the previous chapters. This synthesis focuses on the broad implications of, and applications for, the research completed herein, including suggested applications of refined methodologies, and approaches for future glacier monitoring on the scale of individual glaciers to mountain ranges.

2. An evaluation of mass balance methods applied to Castle Creek Glacier, British Columbia, Canada

Publication details:

This chapter is 'in press' for publication in Journal of Glaciology. Please see Appendix A: Authorship Statements for details of the contributions of each author.

Beedle, M. J., Menounos, B. and Wheate, R. *in press*. An evaluation of mass balance methods applied to Castle Creek Glacier, British Columbia, Canada. *Journal of Glaciology*

2.1. Abstract

I estimate glacier mass balance for years 2009, 2010, and 2011 for a 9.5 km^2 mountain glacier using three approaches. The photogrammetric, global positioning system (GPS), and glaciological methods yielded sampling densities of 100, 5 and 2 points km^{-2} with measurement precisions of ±0.40, ±0.10, and ±0.10 m water equivalent (w.e.) respectively. My glaciological measurements likely include a positive bias, due to omission of internal and basal mass change, and error in determining the interface between snow and firn with a probe (±0.10 m w.e.). Measurements from my photogrammetric method include a negative bias introduced by the manual operator and my temperature index model used to correct for different dates of imaging (0.15 m w.e.), whereas GPS measurements avoid these biases. The photogrammetric and GPS methods are suitable to estimate glacier-wide annual mass balance, and thus they provide a

valuable measure that is complementary to the glaciological method. These approaches, however, cannot be used to estimate mass balance at a point or mass-balance profiles without a detailed understanding of the vertical component of ice velocity.

2.2. Introduction

Geodetic estimates of glacier mass balance quantify changes in surface elevation over a given time period and employ density assumptions for snow and ice. Most geodetic studies assess mass change over periods of a decade or more (e.g., Arendt et al., 2002; Schiefer et al., 2007). Some studies, however, have used geodetic methods to determine mass balance on shorter temporal scales. Meier and Tangborn (1965), for example, used aerial photography taken three years apart to estimate annual mass balance and to investigate short-term ice dynamics of South Cascade Glacier, Washington. Tangborn et al. (1975) made repeat field survey measurements of a 112-point grid on South Cascade Glacier during one ablation season. They found that their geodetic measurements were similar to the glaciological method. Rasmussen and Krimmel (1999) used aerial photogrammetry to derive annual specific mass balance over a portion of South Cascade Glacier for balance years 1993 and 1994. They demonstrated the utility of geodetic measurement, but also identified potential systematic biases in both geodetic and glaciological mass-balance measurements. Krimmel (1999) presented a comparison of South Cascade Glacier annual mass balance derived from both glaciological and photogrammetric methods for 12 balance years (1986-1997). The South Cascade Glacier cumulative geodetic balance was more negative than glaciological balance by about 0.25 m water equivalent (w.e.) a^{-1}, indicative of bias in one or both methods, and possibly due

to basal melt, density estimates, and stakes melting into the glacier surface. The study concluded that photogrammetry can be used to determine annual mass balance if geodetic control is consistent for stereo models.

In the late-1990s, global positioning systems (GPS) were tested as a method to estimate mass balance (Eiken et al., 1997; Gandolfi et al., 1997; Jacobsen and Theakstone, 1997). These studies demonstrated the potential of using GPS in kinematic mode, whereby point measurements are made continuously at a preset time interval, to record glacier surface elevation. Without using real-time kinematic (RTK) GPS, where a real-time differential correction is received from the base station through radio transmission allowing centimeter accuracy, however, these early studies were only able to re-occupy points on a glacier to within tens of meters. Hagen et al. (1999) used GPS to estimate mass balance of Kongsvegen, Svalbard for the period 1991-1995 and found that the results fit well with field measurements of a glacier with negligible vertical velocity. Previous work noted the rapidity and accuracy of kinematic GPS measurements, which might lead to an increase in the number of monitored glaciers (Hagen et al., 1999; Theakstone et al., 1999). Hagen et al. (2005) presented multi-year comparisons of GPS profiles along central flowlines of three Svalbard glaciers. They concluded that changes in glacier geometry cannot be used to assess mass balance without independent knowledge of vertical velocity. In this study, RTK GPS was not used and re-occupation of previously measured points was made only to within 30-90 meters. Other studies have used RTK GPS to accurately re-occupy and re-measure survey points on a glacier to assess multi-year mass balance (e.g., Nolan et al., 2005).

In this chapter I compare glaciological, photogrammetric, and RTK GPS methods to estimate annual glacier mass balance. My objectives are to: 1) test the RTK GPS method; 2) investigate potential error in the glaciological method by comparison with two geodetic methods; and 3) to make recommendations for future mass balance monitoring.

2.3. Theory: Conservation of mass and vertical velocity

Geodetic measurements of glacier thickness change incorporate two dominant terms, surface mass balance and the vertical component of ice flow, necessitating consideration of flux divergence. Conservation of mass at a point on the surface of a glacier (in ice equivalent units, ice eq.) can be stated as:

$$\dot{h} = \frac{\dot{b}}{\rho} - \nabla \cdot \vec{Q} \tag{2.1}$$

where $\dot{h}$ is the rate of thickness change, $\dot{b}$ is the specific surface mass balance rate, ρ is density of the surface material relative to water, and $\nabla \cdot \vec{Q}$ is a flux-divergence term (e.g., Rasmussen and Krimmel, 1999; Cuffey and Paterson, 2010). Implicit in Eqn (2.1) are the assumptions that densification, internal and basal mass changes, isostatic displacement, and erosion of the bed surface are all negligible. When integrated across the entire glacier surface, and assuming a negligible influence from changing surface area and no flux across the glacier boundary (e.g., from avalanching or calving), flux divergence is zero, yielding:

$$\dot{H} = \frac{\dot{B}}{\rho} \tag{2.2}$$

where $\dot{H}$ and $\dot{B}$ are glacier-wide integrations of thickness change and surface mass balance respectively.

Flux divergence, however, is not zero for a given point, and the vertical component of ice velocity at the surface (vertical velocity, w_s) plays a confounding role in deriving $\dot{b}$ from measurements of $\dot{h}$. Previous studies use Eqn (2.1) to estimate $\dot{b}$ from geodetic measurements and include a complete treatment of the flux divergence term in Eqn (2.1), with consideration of the vertical profile of velocity and the component of surface flow due to sliding (e.g., Gudmundsson and Bauder, 1999; Rasmussen and Krimmel, 1999).

In studies to quantify w_s, some efforts include consideration of sub-surface glacier flow or assume steady-state conditions (e.g., Reeh et al, 1999; Reeh et al., 2003), while others neglect the vertical profile of velocity (e.g., Meier and Tangborn, 1965; Holmlund, 1988; Pettersson et al., 2007), and rely on the kinematic boundary condition at the glacier surface:

$$\dot{h} = \frac{\dot{b}}{\rho} + w_s - u_s \frac{\partial S}{\partial x} - v_s \frac{\partial S}{\partial y} \tag{2.3}$$

where u_s and v_s are the horizontal components of ice velocity at the glacier surface S (Cuffey and Paterson, 2010). Often, Eqn (2.3) is used to estimate w_s in only the ablation zone and is further reduced to a simple geometric expression (e.g., Meier and Tangborn, 1965; Holmlund, 1988; Pettersson et al., 2007):

$$w_s = \dot{h} + u_s \tan\alpha \tag{2.4}$$

where $\dot{h}$ is thickness change measured at a marker (usually a stake) moving with glacier flow, u_s is oriented along the flow, v_s is assumed to be zero, and α is surface slope (Cuffey and Paterson, 2010).

Previous work that employs either Eqn (2.1) to estimate $\dot{b}$ from geodetic measurements, or Eqns (2.3) and (2.4) to estimate w_s relies on a Lagrangian frame of reference, whereby horizontal flow and occasionally $\dot{h}$ are measured at a marker, such as a stake, as it moves with the ice. In an Eulerian frame of reference, where measurements are made at fixed coordinates, $\dot{h}$ changes as the sum of $\dot{b}$ and w_s (Cuffey and Paterson, 2010). However, horizontal ice flux at the surface (u_s and v_s in Eqn (2.3)) advects glacier surface topography through locations where geodetic repeat measurements are made. I discuss this as a source of error below, but otherwise neglect advection of topography in my geodetic measurement of mass balance and estimation of w_s. Omission of these horizontal velocity terms yields:

$$\dot{h} = \frac{\dot{b}}{\rho} + w_s \tag{2.5}$$

which may be rearranged to solve for specific mass balance:

$$\dot{b} = \left(\dot{h} - w_s\right)\rho \tag{2.6}$$

or for vertical velocity:

$$w_s = \dot{h} - \frac{\dot{b}}{\rho} \tag{2.7}$$

In addition to advection of topography, Eqns (2.5-2.7) also neglect densification, internal and basal mass balance, isostatic displacement, and erosion of the bed surface.

Vertical velocity at the surface (w_s) is typically negative or downward (submergence) in the accumulation zone and positive or upward (emergence) in the ablation zone. To avoid ambiguity in my discussion of these, I use the term emergence to refer to positive (upward) flow, submergence to refer to negative (downward) flow, and vertical velocity as a general term without a specified sign.

2.4. Methods

I measured mass balance of Castle Creek Glacier, in the Cariboo Mountains of British Columbia, Canada (Beedle et al., 2009). This 9.5 km^2 mountain glacier flows north for 5.9 km, has an elevation range of 2,827 to 1,810 m above sea level (asl), and contributes meltwater to Castle Creek, a tributary of the Fraser River (Fig. 2.2).

My terminology and notation follow the recommendations of Cogley et al. (2011). The glaciological method measures surface mass balance, whereas the two geodetic estimate mass change from measurements of elevation change, which includes surface, internal and basal ablation and accumulation. For simplicity, however, I refer only to annual mass balance regardless of method. A mass-balance profile, $b(z)$, is defined as the variation of mass balance with elevation. I use dh as notation for thickness change, and $dh(z)$ to refer to the profile of thickness change with elevation. All measurements of glacier-wide mass balance presented are conventional balances whereby values are averaged over a changing glacier surface (Elsberg et al., 2001), allowing direct comparison of glaciological and geodetic methods. The changing ice geometry is based on digital elevation models (DEMs) from 2008, 2009, and 2011 aerial

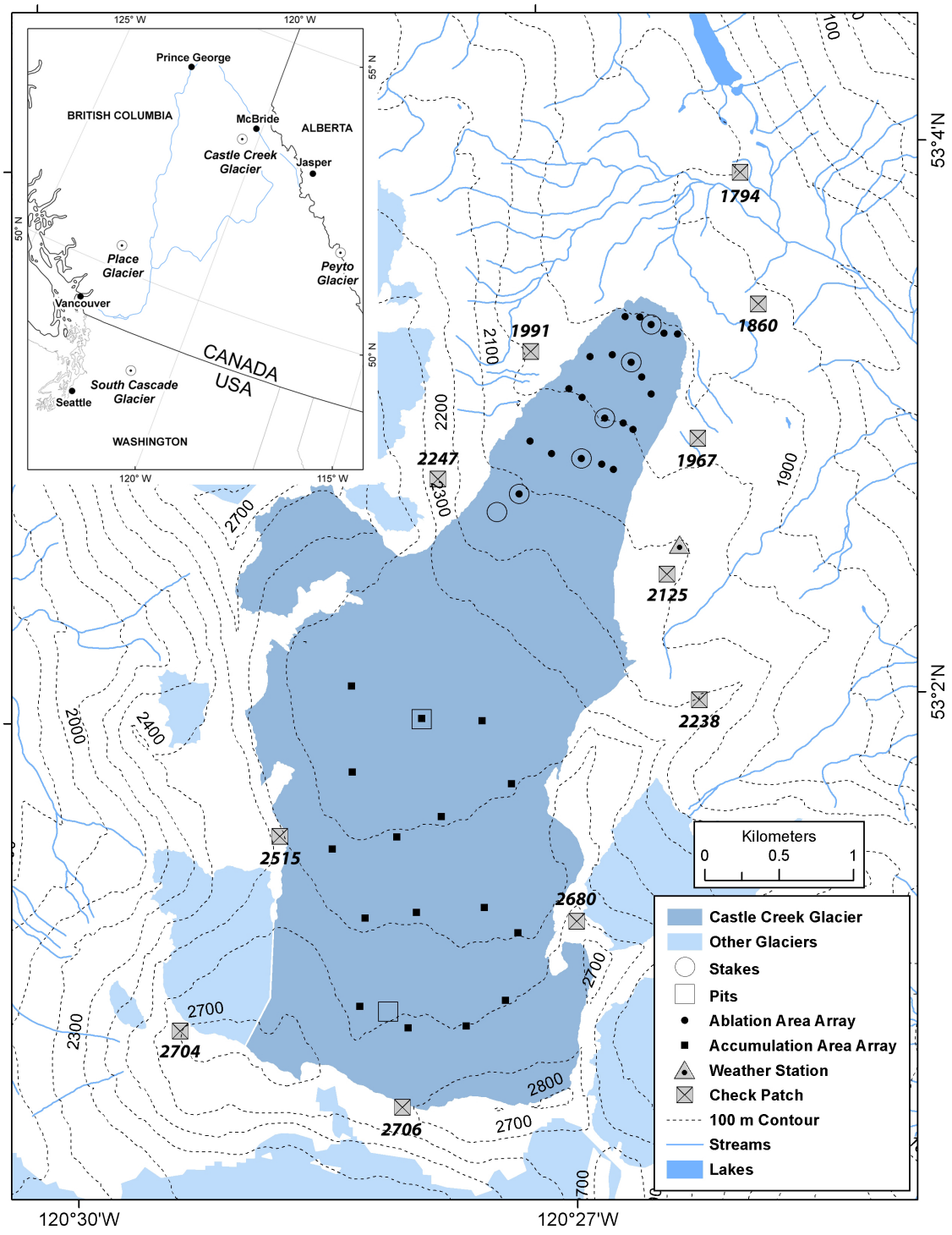

Figure 2.1 Location of Castle Creek Glacier and nearby glaciers with reference mass-balance series (inset). The inset also includes nearby towns, major cities and two main stems of the Fraser River, into which Castle Creek Glacier meltwater flows. Check patches are labeled by their respective mean elevation.

photos. I estimate the 2010 glacier geometry by linear interpolation from the 2009 and 2011 DEMs. Castle Creek Glacier surface areas used to convert from volume change to specific (per unit area) mass balance are 9.56 (2009), 9.52 (2010), and 9.49 km^2 (2011).

2.4.1. Glaciological method

Snow pits and probing are used to directly measure accumulation, whereas stakes measure surface ablation (e.g., Østrem and Brugman, 1991; Kaser et al., 2003). I use the stratigraphic system to define the annual mass balance, whereby measurements are made between successive annual minima, typically in early-September at Castle Creek Glacier. Conversion to w.e. is made by assuming ice density to be 900 kg m^{-3}, and from snow density measured in snow pits. Measured snow density at the end of the ablation season is less spatially variable than snow depth, with relative standard deviations of <1% and 33% respectively. Point measurements of mass balance (b_a) were made at 21, 12, and 18 sites during the balance years of 2009, 2010 and 2011, equating to sampling densities of 2.2, 1.3, and 1.9 points km^{-2} respectively. Glaciological measurements are absent for a portion of the middle of the glacier where an icefall impedes safe travel.

I apply the balance-gradient (or regression) method to extrapolate from b_a measurements to glacier-wide annual mass balance (B_a), using surface area defined by 50 m elevation intervals (e.g., Fountain and Vecchia, 1999). For the glaciological method, I use a three-part linear spline to represent the variation of b_a with elevation. This spline is derived from the b_a measurements, with the intercept set to the observed elevation of the annual snowline ($b_a = 0$). My measurements do not reach the highest elevation bins of Castle Creek Glacier; I apply the measurements from my highest measurements to these

Table 2.1 Aerial photography and stereo model details. GCP, as used in column eight, is an acronym for ground control point.

Date	Camera/media	Band	Focal Length (mm)	Scale	Image Pixel Size (μ)	Ground Sampling Distance (m)	RMS of GCP Positions x,y,z (m)	Surface Contrast
2008-08-16	Wild RC30 (Film)	Visible	152.819	1:20,000	12 (scanned)	0.25	0.242, 0.242, 0.058	Good
2009-08-07	Wild RC30 (Film)	Visible	152.819	1:20,000	12 (scanned)	0.25	0.258, 0.206, 0.067	Good
2011-09-03	UltraCam X (Digital)	Near infrared	100.5	1:25,000	21.6	0.53	0.179, 0.223, 0.021	Poor

uppermost elevation zones of the glacier (e.g., Cogley et al., 1996). Use of a linear spline to interpolate from mass-balance observations has been found to be similar to a quadratic interpolation and superior to the contour method (Fountain and Vecchia, 1999).

2.4.2. Photogrammetric method

I use aerial photographs taken in 2008, 2009 and 2011 to derive B_a for 2009, and cumulative balances for the periods 2008 – 2011, and 2009 – 2011 (Table 2.1). Ground sampling distance of the 2008 and 2009 images is 0.25 m, and 0.53 m for the 2011 images. Ground control points (GCPs) were obtained from stereo models of 2005 aerial triangulation scans made available by the Province of British Columbia.

I created stereo models from photography using the Vr Mapping photogrammetry software suite (Cardinal Systems LLC). A common set of 18 GCPs, consisting of bedrock features or stable boulders distributed around the glacier at various elevations and 50-70 tie points were used for exterior orientation and generation of stereo models (e.g., Schiefer and Gilbert, 2007; Barrand et al., 2009). The use of the same GCPs for all years ensured that positional errors were randomly distributed (Kääb & Vollmer, 2000; Schiefer and Gilbert, 2007; Schiefer et al., 2007). Analysis of 11 check patches allows me to measure the relative accuracy and assess systematic bias between stereo models. These check patches consist of 25 individual check points in a 5 m grid, located on stable

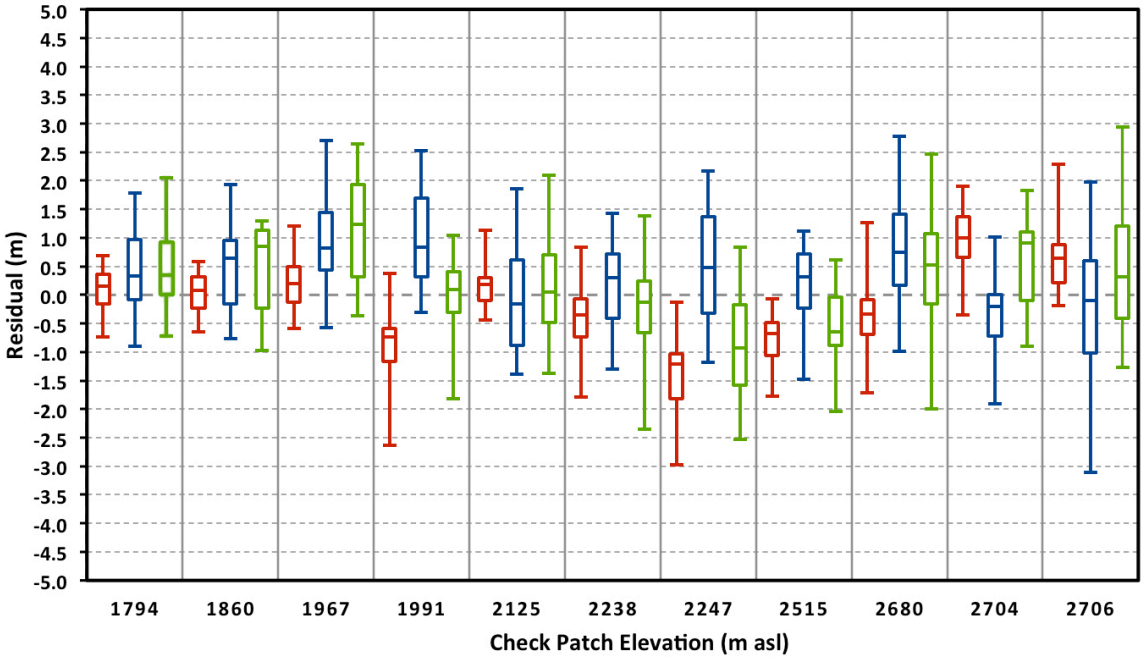

Figure 2.2 Elevation residuals of check patches collected from three different stereo models. Each boxplot displays the distribution of surface-elevation residuals of 25 check points, defined as the difference in surface elevation of the same horizontal coordinates from the first stereo model to the second in a given epoch. The three boxplots for each check patch show residuals for the epochs 2008 - 2009, 2009 - 2011, and 2008 – 2011 respectively from left to right. See figure 2.1 for check-patch locations.

bedrock near the glacier (Figs. 2.1 and 2.2). I estimated systematic bias among stereo models and derived trend surfaces based on the mean residuals of the 11 check patches; these trend surfaces were then used to apply a correction for elevation points on the glacier. I also compared the average slope angle of each check patch with the mean residual of the 25 individual points to detect any horizontal bias among models.

To map glacier surface elevation, I manually digitized mass points (series of *x,y,z* data points collected on a predetermined grid) on a 100 m grid within the glacier extent as manual measurements yield results superior to automated extraction methods (McGlone et al., 2004). Good contrast in the 2008 and 2009 photography enabled me to

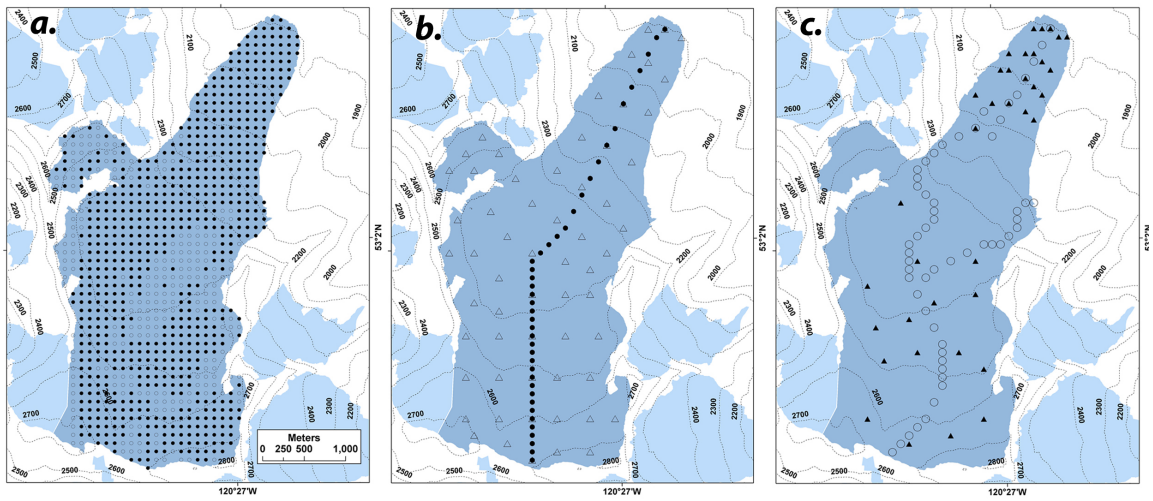

Figure 2.3 (A) Grids of photogrammetric mass points for 2011 (black dots) and 2008 and 2009 (black dots and open circles), (B) subsets of mass points for "long profile" (black dots) and "grid" points (open triangles), and (C) "walkable routes" (open circles) and "arrays" (black triangles).

measure every grid point (n = 937), but poor photographic contrast due to fresh snow cover in the 2011 photography reduced measurements by 26% (Fig. 2.3).

The largest source of error in my photogrammetric methodology is my ability to perceive and measure the glacier surface, a methodological shortcoming noted by others (e.g., Rasmussen and Krimmel, 1999). This bias decreased with repeated measurements (Fig. 2.4). I define blunders as points that fall outside 68% (± 1σ) of measured elevation change for a given 50 m elevation interval, and I re-measured blunders five times for the 2008 and 2009 models, and three times for the 2011 models. To correct persistent blunders (<5%), I performed ordinary kriging interpolation from the non-blunder mass points, and extracted elevations from these trend surfaces.

As the photograph dates did not match the date of field measurements, I made corrections using a temperature-index model (Hock, 2003). I derived glacier surface temperature for the model from observations at an automated weather station near the east margin of the glacier (2105 m asl, Fig. 2.1), which is outside the influence of

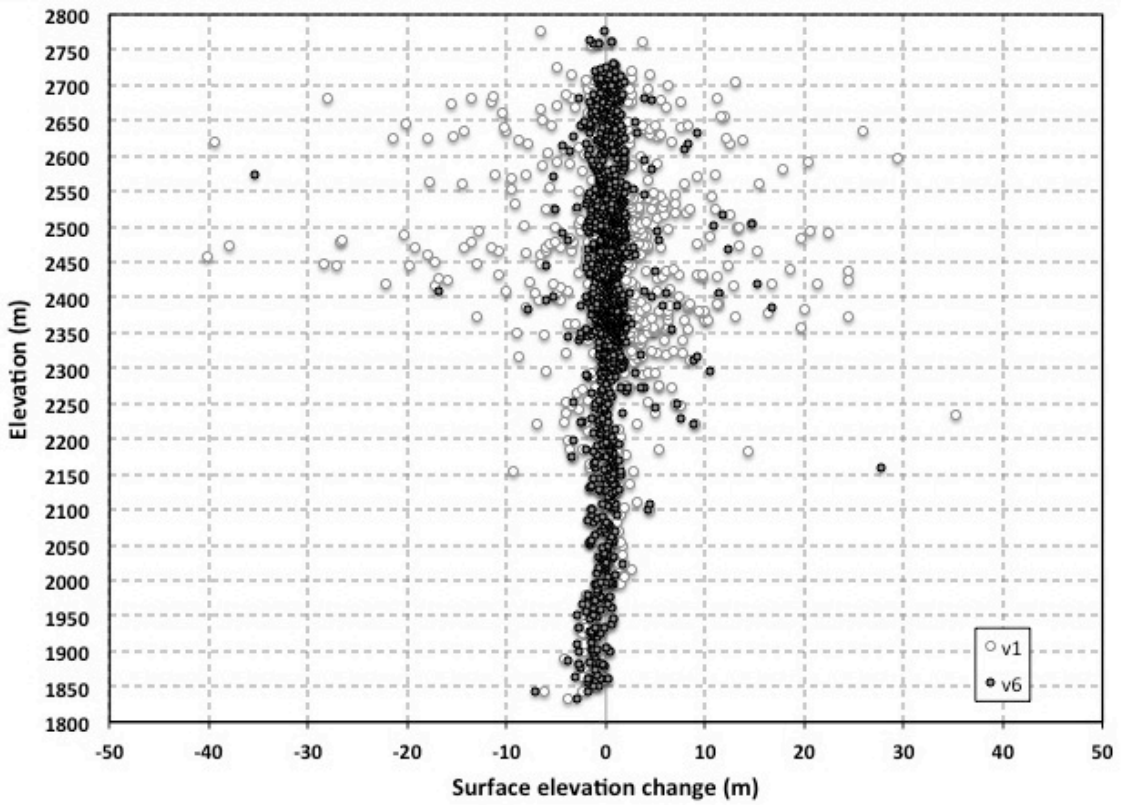

Figure 2.4 Thickness change for balance year 2009 from manual aerial photogrammetry. The two sets of mass points are from the first (v1) and sixth (v6) measurements of mass points, illustrating improved performance of the photogrammetrist.

katabatic winds (Déry et al., 2010). I assume a lapse rate of 0.006 ºC m^{-1}, apply melt factors derived from mass-balance data (Shea et al., 2009) for Place Glacier (k_s = 2.76, k_i = 4.67), and compare my findings to results using melt factors from Peyto Glacier (k_s = 2.34, k_i = 5.64) and my more limited observations at Castle Creek Glacier (k_s = 3.45, k_i = 4.33).

Geodetic mass-balance methods necessitate assumptions of the density of ice and snow lost or gained from the surface of a glacier (e.g., Huss, 2013). I tested three scenarios to assess my density assumptions: the first scenario (A) assumes that the density profile of the glacier remains unchanged with time (Sorge's law; Bader, 1954) and 900 kg m^{-3} is used to convert from ice eq. to w.e. My second scenario (B) uses 900

kg m^{-3} for all points below the equilibrium line altitude (ELA), and 750 kg m^{-3} for all points above the ELA – assuming that the loss or gain of material in the accumulation zone is not entirely composed of ice, but at least partially of firn and snow (e.g., Zemp et al., 2010). The third scenario (C) uses 900 kg m^{-3} for all points below the ELA, and 600 kg m^{-3} for all points above the ELA – assuming that the loss or gain of material in the accumulation zone has a density equivalent to end-of-season densities measured in my snow pits. These three scenarios use maps of accumulation and ablation zones based on glacier extent and observations of the ELA in the latter year of each period. Average glacier-wide densities for Castle Creek Glacier elevation change vary from 800-850 kg m^{-3} for B, and from 699-726 kg m^{-3} for C.

To calculate B_a via the photogrammetric method, I use two methods of spatial extrapolation. For balance year 2009, when the 100 m grid is measured in its entirety, I apply the arithmetic mean of all 937 points. This assumes that all vertical velocities sum to zero (Eqn 2.2). The second method sums the product of the average $dh(z)$ from each 50 m elevation interval and its surface area. In this second method, the integral of the emergence velocities from the subset of points might be zero (e.g., along a flowline; Cogley, 2005), or non-zero, introducing an error or bias in the estimate of B_a.

2.4.3. RTK GPS method

To perform RTK GPS surveys (hereafter denoted as GPS) I used Topcon GB-1000 dual-frequency receivers (measurement precision of ±0.03 m). Re-occupation of previously measured points indicated a horizontal accuracy of ±0.03 m, and repeat measurements of three check points on stable bedrock respectively indicated horizontal

and vertical accuracy of 0.02 ± 0.01 m and 0.03 ± 0.02 m. I attached the rover antenna to a short antenna pole that was in turn attached to my backpack. The distance from the rover antenna to the glacier surface was measured on a flat surface and assumed to be constant (e.g., Nolan et al., 2005).

I made measurements of *dh* via GPS along longitudinal profiles and at grid points (Figs. 2.1 and 2.3). For initial measurement of the longitudinal profiles, I collected points in kinematic mode at 5 s intervals and differentially corrected these points. From these kinematic profiles I selected points every 10 m in elevation for GPS measurement in successive years. I established grids of points on cross-glacier profiles at common elevations, yielding 20 points in the ablation zone and 16 points in the accumulation zone (Fig. 2.1).

Calculated *dh* was converted to w.e. using the three density scenarios discussed above. GPS measurements were made at the same time as the glaciological measurements and thus no melt correction was needed between them. Unfortunately, poor line of sight with the base station and insufficient base radio power resulted in few measurements in the accumulation zone and I thus adopt the balance-gradient method to achieve B_a using a linear spline and the period-specific hypsometry. For GPS measurements, I use a two-part linear spline fit to my 2011 observations (Fig. 2.5). This spline is then shifted to match 2009 and 2010 ablation-zone b_a measurements. With this shift I assume the profile shape does not change from year to year, and that few lower-elevation observations can be used to adequately define $b(z)$ (e.g., Rasmussen and Krimmel, 1999).

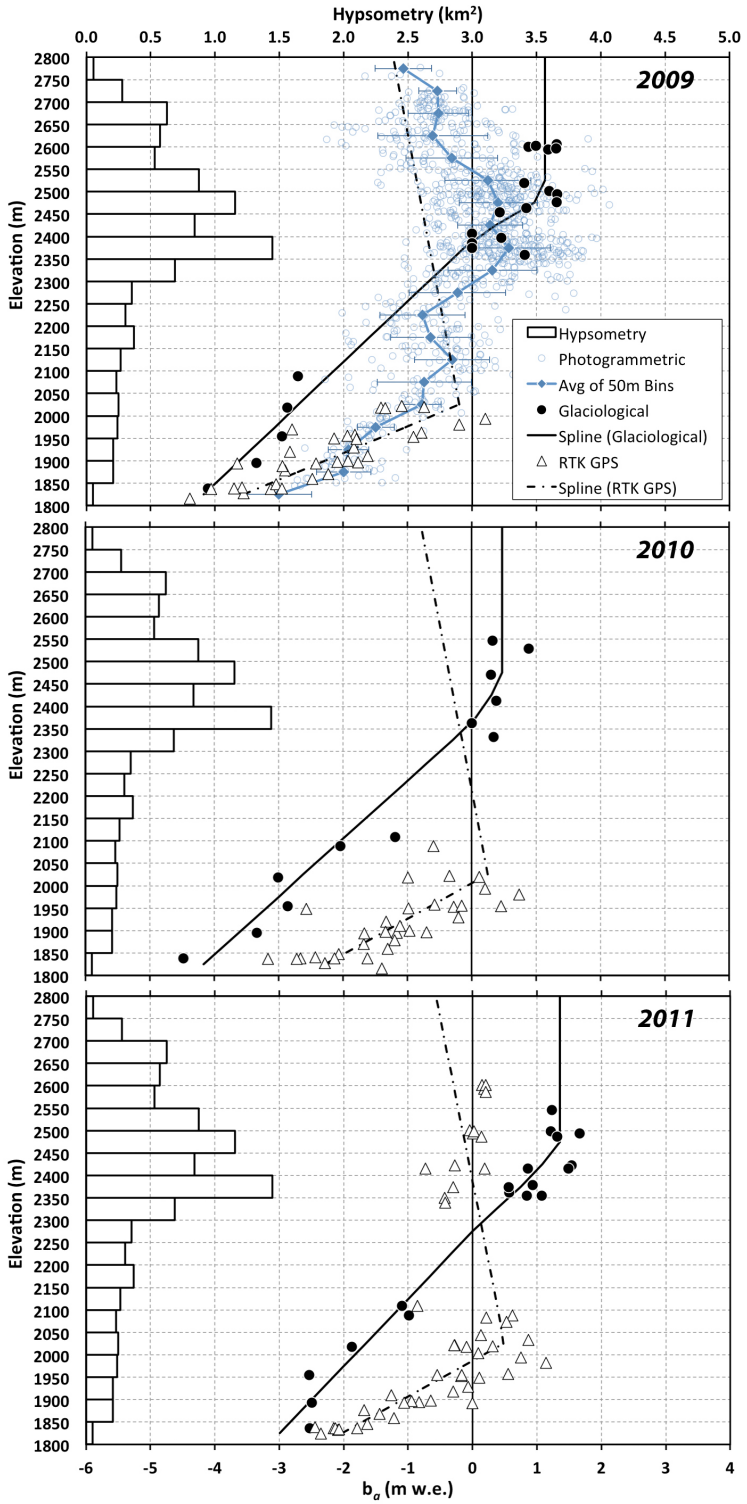

Figure 2.5 Measurements of at-a-point mass balance and thickness change, and associated profiles with elevation, for balance years 2009, 2010 and 2011. Spatial extrapolation uses the hypsometry displayed at left. Error bars in the top panel indicate 1σ of the photogrammetric measurements within each 50 m elevation bin.

Additionally, I tested the sensitivity of using fewer, GPS measurements to estimate B_a by using four different subsets of the 937 photogrammetric measurements for balance year 2009 (Fig. 2.3). These subsets include: 1) a "long profile" of 41 points along the glacier center-line, 2) "walkable routes" consisting of 56 points, which are the safely navigable routes of my GPS longitudinal-profiles, 3) "arrays" consisting of the 36 ablation and accumulation zone points measured *in situ*, and 4) a "grid" consisting of 61 points, regardless of safe travel.

2.4.4. Estimation of vertical velocity

I employed an Eulerian frame of reference to estimate vertical velocity at fixed coordinates using Eqn (2.7) with GPS measurements of $\dot{h}$ and glaciological measurements of $\dot{b}$. From August to September (2008-2010), I estimated vertical velocity for point arrays in the ablation and accumulation zones of Castle Creek Glacier (Fig. 2.1). I placed twenty ablation stakes (ablation array) in four across-glacier profiles. At each stake, which typically travelled 5-20 m a^{-1} down glacier, I measured surface ablation; *dh* was measured with GPS at fixed coordinates where stakes were initially placed. I assume that ablation measured at a transient stake is representative of ablation at the site where it was initially placed.

To estimate vertical velocity in the accumulation zone I made four probing observations within 3 m of the location where surface elevation was measured with GPS. The average of these multiple observations was used to minimize errors stemming from a non-vertical probe, the observer's ability to accurately probe the previous summer surface, and the effects of meter-scale variability in the summer surface (e.g., from sun

cups, meltwater channels, and differential ablation). I assume that the difference between probing observations at successive times is representative of b, even though horizontal flow in the period between the two observations (2 - 10 m) results in a different snowpack and surface being probed. Complications with GPS radio transmission reduced my initial 16-point accumulation array to seven observations in one August to September period (2009).

I compare these estimates of vertical velocity made at fixed coordinates (Eulerian frame of reference) with those from the often-used geometric relation at the surface (Eqn (2.4)) made at a stake (Lagrangian frame of reference). I employ Eqn (2.4) with GPS measurements of $\dot{h}$ made at stakes, and α derived from a common DEM.

2.5. Error analysis

My error analysis assumes all compounded error terms are uncorrelated. Error estimates in my measurement of cumulative mass balance from glaciological and GPS methods likewise assume annual measurements are uncorrelated.

2.5.1. Glaciological method

Many studies have reported a random error of ±0.20 m w.e. a^{-1} for b_a, and this estimate is often taken to be a reliable estimate of B_a uncertainty given the spatial autocorrelation of mass balance measurements (Cogley and Adams, 1998). Recent re-analysis of glaciological measurements finds that this error is ±0.34 m w.e. a^{-1} (Zemp et al., 2013). A major source of error in glaciological mass balance measurements is the spatial variability of b_a (e.g., Kaser et al., 2006). I quantify random error in my

glaciological measurements from uncertainties in the measurements and their extrapolation. Random errors from stake measurements arise from the determination of the surface due to surface roughness and ablation caused by the stake and average ±0.10 m w.e. a^{-1} (e.g., Huss et al., 2009); I adopt this error term as it accords with my observations.

Accumulation measurements rely on depth and density measurements in pits and depth measurements by probing. Measurement errors of snow depth include misidentification of the previous year's surface and determination of the undulating present-year surface; pit measurements are less problematic than soundings with a probe. Penetration by a probe into underlying firn would overestimate mass balance (Thibert et al., 2008). I found that misidentification of an overlying ice lens as the previous year's surface was as common as probing into the underlying firn, and treated it as a random error term instead of a bias. Deviation of a probe from vertical, however, overestimates snow depth and introduces a positive bias (Østrem and Haakensen, 1999). Over three balance years I probed snow depth at 98 sites; I probed snow depth in the four cardinal directions around each site. The average standard deviation of these 392 probing observations was 0.07 m ice eq. Many studies estimate the compounded random error of accumulation measurements (typically ±0.30 m w.e. a^{-1}) to be greater than those from the ablation zone, (e.g., Huss et al., 2009). However, my average standard deviation of 0.07 m ice eq. from four probing measurements at 98 locations suggests a reduced error. I use an error estimate of ±0.10 m ice eq. a^{-1} for all stake, pit, and probing measurements of ablation or accumulation depth.

Errors in measurements of b_a also arise from an assumption of the density of ice (900 kg m^{-3}) and the measurement of snow density in pits. I used a large 500 cm^{-3} tube core for the purpose of sampling snow within pits. Snow cutters have a typical measurement error of 11%, and the larger tube cutters are of higher precision (Conger and McClung, 2009). My field scale has a measurement error of ±3.3%, or ±10 grams for an average sample weight of 300 grams. I thus conservatively assume an error in my accumulation zone density measurements of 10%, or ±60 kg m^{-3} for average conditions in my three years of study.

I therefore estimate error in b_a as:

$$\sigma_{b_a} = \sqrt{\sigma_l^2 \rho^2 + \sigma_\rho^2 l^2} \qquad (2.8)$$

where σ_l is the estimated error in my measurements of the length of ablation and accumulation (±0.10 m ice eq. a^{-1}), l is an area-weighted average ablation and accumulation measurement (2.0 m ice eq. a^{-1}), σ_ρ is an area-weighted average of error in density assumptions and measurements expressed as a conversion factor (±0.04), and ρ is an area-weighted density expressed as a conversion factor (0.72).

I calculate sampling error - extrapolation from $b(z)$ to B_a via the hypsometry - by the standard deviation of the residuals between my observations and the linear spline. These residuals are 0.36, 0.37, and 0.25 m w.e. for balance years 2009, 2010, and 2011 respectively.

Error in planimetric area (Granshaw and Fountain, 2006; Bolch et al., 2010), defined as the sum of squared horizontal error in stereo model registration and digitizing

error (±5 pixels), yields ±0.3% for balance years 2009 and 2010, and ±0.6% for balance year 2011.

Measurement and extrapolation errors for each balance year are thus:

$$\sigma_{Glac} = \sqrt{\sigma_{b_a}^2 + \sigma_{Ext}^2} \tag{2.9}$$

where σ_{Glac} is the estimated error for glaciological B_a, σ_{b_a} is measurement error, and σ_{EXT} extrapolation error.

2.5.2. Photogrammetric method

I quantify the uncertainty in *dh* using the standard deviation of elevation residuals of 275 points in 11 check patches (Figs. 2.1 and 2.3). These residuals reveal the combined error in my stereo models (*x,y,z*) and my precision and accuracy in manually digitizing points (*z*). I follow Rolstad et al. (2009) to assess uncertainty in sequential DEM analysis when the correlation range - the extent of spatial autocorrelation - is less than the averaging area:

$$\sigma_A^2 = \sigma_{\Delta z}^2 \frac{1}{5} \frac{A_{cor}}{A} \tag{2.10}$$

where σ_A^2 is the variance of the spatially averaged elevation difference, $\sigma_{\Delta z}^2$ is the variance of the elevation difference, A_{cor} is the correlation area, and A is the glacier surface area.

I calculate A_{cor} (Rolstad et al., 2009) as:

$$A_{cor} = \pi a_1^2 \tag{2.11}$$

where a_1 is the correlation range determined using the Incremental Spatial

Autocorrelation tool in ArcGIS 10.1, which gives the Global Moran's I statistic over a series of increasing distances (e.g., Getis and Ord, 1992).

For all geodetic measurements of B_a presented below, I convert to w.e. using my B scenario that assumes 900 kg m^{-3} for all points below the ELA, and 750 kg m^{-3} for all points above the ELA. To quantify error in this density assumption I use a range of possible density values, with the maximum density error defined by the A scenario, which assumes a density of 900 kg m^{-3} for all points. The minimum density is defined by the C scenario, which assumes 900 kg m^{-3} below the ELA and 600 kg m^{-3} above the ELA. I consider these extrema as the plausible range of densities (±3 s) and use these as a conservative estimate of density-assumption error.

I propagate the DEM error and density-assumption error as:

$$\sigma_{B_p} = \sqrt{\sigma_A^2 \rho^2 + \sigma_\rho^2 A^2} \tag{2.12}$$

where σ_{B_p} is the error in my photogrammetric B_a measurements (m w.e. a^{-1}), σ_A is the DEM error (0.30 m ice eq.) , A is area-weighted surface thickness change (1.00 m ice eq. a^{-1}), σ_ρ is my estimate of density-assumption error from a range of possible values expressed as a conversion factor (±0.09), and ρ is an area-weighted density expressed as a conversion factor (0.81).

To estimate error in my correction for differing observation dates, I use the standard deviation of the residuals of measured and modeled ablation from my mid-summer array measurements. The total number of array points is 71 from 2008, 2009, and 2010, but most of these points (64) are in the ablation zone. Residuals from all points have a mean of -0.01 m ice eq. and a standard deviation of 0.20 m ice eq.

However, the seven points from the accumulation zone have a residual mean of -0.24 m ice eq., which indicates there is a potential systematic bias in my date correction.

I estimate error in my date-corrected photogrammetric B_a measurements (σ_{Phtgrm}) as:

$$\sigma_{Phtgrm} = \sqrt{\sigma_{B_p}^2 + \sigma_{Corr}^2} \quad (2.13)$$

where σ_{B_p} is the error in my photogrammetric B_a measurements (Eqn (2.12)), and σ_{Corr} is the estimated error in my correction for differing observation dates.

2.5.2. GPS method

The random error in *dh* arises from movement of the antenna attached to my pack, my stance on an uneven surface, and foot or ski penetration into a firn or snow surface. I thus adopt a conservative measurement error of ±0.10 m (e.g., Nolan et al., 2005), which is three times greater than the measurement error (±0.03 m) I observed by resurveying benchmarks.

For GPS measurements, I employ the same density assumptions and error estimates as my photogrammetric approach. As with my glaciological measurements, I estimate error in specific GPS measurements (b_{GPS}) as:

$$\sigma_{b_{GPS}} = \sqrt{\sigma_h^2 \rho^2 + \sigma_\rho^2 h^2} \quad (2.14)$$

where σ_h is the estimated error in my measurements of thickness change (±0.10 m ice eq. a^{-1}), h is an area-weighted average measurement of thickness change (-0.70 m ice eq. a^{-1}), σ_ρ is an area-weighted average of error in density assumptions and measurements

expressed as a conversion factor (±0.09), and ρ is an area-weighted density expressed as a conversion factor (0.81).

GPS interpolation error is approximated by the standard deviation of the residuals between my observations and the linear spline. I use ±0.57 m to estimate sampling error for all three balance years; this value arises from measurements made in 2011 which included the accumulation area.

The estimated error for the GPS method is:

$$\sigma_{GPS} = \sqrt{\sigma_{b_{GPS}}^2 + \sigma_{Ext}^2} \tag{2.15}$$

where σ_{GPS} is the estimated error for glacier-wide GPS mass balance (B_{GPS}), $\sigma_{b_{GPS}}$ is measurement error, and σ_{EXT} is extrapolation error.

2.6. Results

The glaciological method yields two years of negative mass balance, followed by a third year of mass gain, resulting in a cumulative balance for the period 2009-2011 of 0.10 ± 0.63 m w.e. (Table 2.2). The photogrammetric result for balance year 2009 (-0.15 ± 0.36 m w.e.) overlaps with the glaciological method (-0.12 ± 0.39 m w.e.). Photogrammetrically-based mass change for the periods 2009 – 2011 and 2010 – 2011, however, are more negative than those derived by the glaciological method (Table 2.2). My GPS-derived mass balance estimates for the year 2010 (-0.34 ± 0.57 m w.e.) and the period 2010-2011 (-0.44 ± 0.81 m w.e.) overlap with the glaciological method (respectively -0.31 ± 0.40 and -0.44 ± 0.26 m w.e.), but the GPS results for balance years 2009, 2011, and cumulative period 2009-2011 are more negative than either the

Table 2.2 Estimates of glacier-wide mass balance (B_a) by the three different methods.

Balance Year	Glaciological (m w.e.)	Photogrammetric (m w.e.)	RTK GPS (m w.e.)
2009	-0.12 ± 0.39	-0.15 ± 0.36	-0.82 ± 0.58
2010	-0.31 ± 0.40	no data	-0.34 ± 0.57
2011	0.53 ± 0.29	no data	-0.10 ± 0.57
2009 - 2011	0.10 ± 0.63	-0.59 ± 0.33	-1.26 ± 0.99
2010 - 2011	0.22 ± 0.49	-0.44 ± 0.26	-0.44 ± 0.81

glaciological or photogrammetric results (Table 2.2). For the period 4 August to 14 September 2009 – an additional period for which I made both glaciological and GPS measurements, with points distributed in both the accumulation and ablation zones – I find similar results of -1.02 ± 0.28 and -0.98 ± 0.28 m w.e.

I tested the reliability of using the reduced subset of photogrammetric points measured in 2011 (n = 698, 74%) to represent glacier-wide elevation change by comparing B_a for the year 2009 derived from 100% of the points with a synthetically thinned subset of points matching the point locations of those measured in 2011. This comparison yielded B_a of -0.15 m for both 100% and 74% coverage, suggesting that incomplete coverage of the glacier in 2011 is likely not the source of differences in the methods.

Using a subset of geodetic point measurements (e.g., via GPS) yielded results comparable to those from measurements across the entire glacier surface (e.g., photogrammetry) if measurements were made in all elevation bins. I measured B_a as -0.08 (n = 41), -0.15 (n = 56), 0.02 (n = 37), and -0.10 m w.e. (n = 61) in four subsets, compared with -0.15 ± 0.36 m w.e. (n = 937) for the 100-m grid covering the entire glacier (Fig. 2.6). The subset with a slightly positive B_a (0.02, n = 37) is the only subset

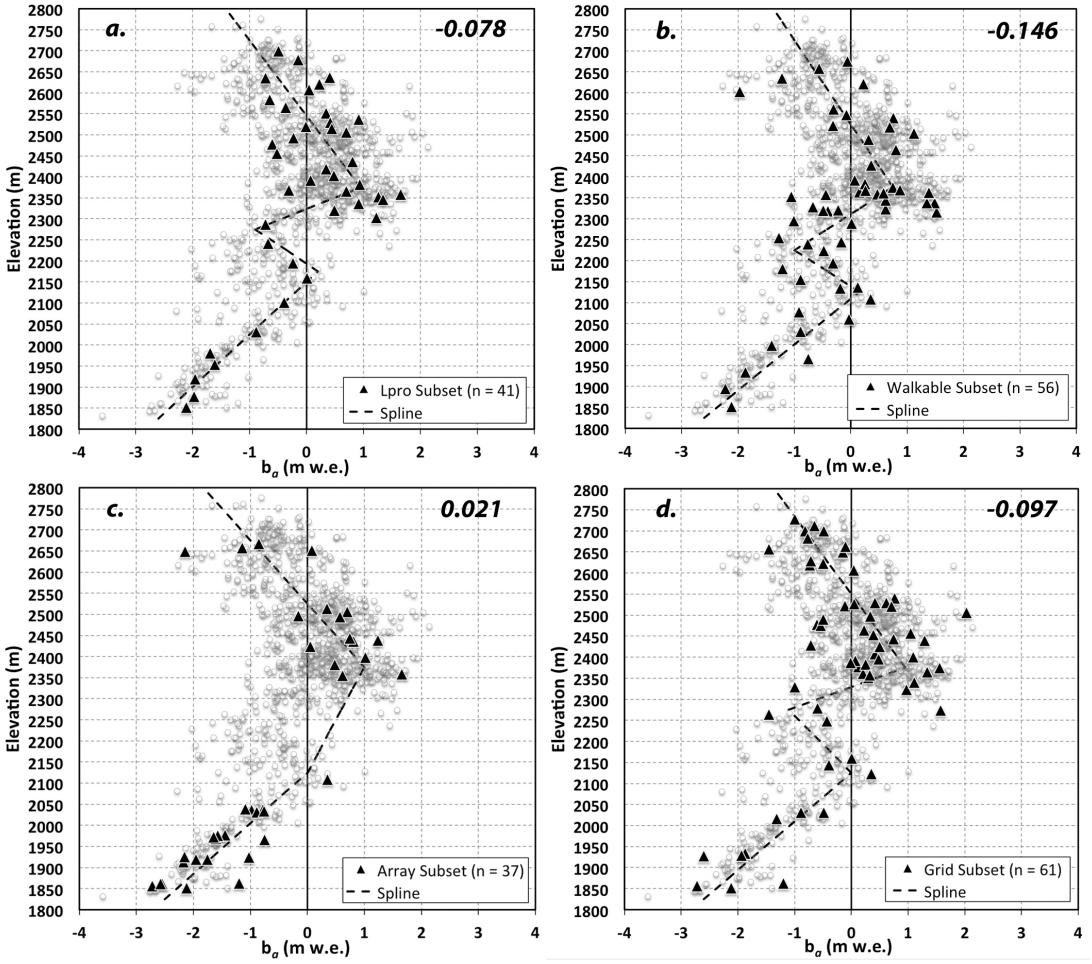

Figure 2.6 Four subsets (triangles) of the 2009 photogrammetric mass points (circles): a) Points on a longitudinal profile along the center of the glacier, b) points along safely walkable longitudinal profiles, c) 37 array-point locations, and d) points from an evenly-spaced grid. Values in the upper right corner of each panel indicate B_a for the associated subset. Spatial locations of each subset are displayed in figure 2.3.

that does not include measurements in all elevation bins, with a data gap over the mid-glacier icefall (Fig. 2.3).

2.6.1. Error

The error (±0.35 m w.e.) in the glaciological measurements is dominated by the spatial variability of b_a. The precision of my accumulation-zone measurements is ±0.10 m, three times more precise than Huss et al. (2009). The coefficient of variation (ratio of standard deviation to mean) of accumulation-zone b_a, however, is twice that of the

ablation zone. The large error term in my glaciological measurements thus arises from the high spatial variability of b_a in the accumulation zone.

Errors in my photogrammetric methodology are dominated by the precision and accuracy of my manual measurements of photogrammetric mass points (DEM uncertainty), and number of independent samples in my sampling grid, which depends on the spatial autocorrelation of the surface elevation data. Photogrammetric measurements of *dh* are five times less precise than either the glaciological or GPS data. Rolstad et al. (2009) found spatial correlation within DEMs generated by automated photogrammetry at three spatial scales: hundreds of meters, a few kilometers, and at tens of kilometers. They hypothesize that correlation at hundreds of meters was the result of matching errors in their automated methodology, whereas correlation at tens of kilometers was due to inaccurate georeferencing. Others (e.g., Nuth et al., 2007; Barrand et al., 2010) have relied on this study to justify an assumption of a correlation area of 1 km^2. These studies use automated techniques to investigate decadal change in contrast to my manual methods to assess annual change. Based on my assessment of correlation range, I estimated values of 1600, 700, and 1100 m in balance year 2009, and periods 2010-2011 and 2009-2011 respectively, resulting in correlation areas of 8.0, 1.5, and 3.8 km^2, which yield more conservative estimates of DEM error than if I had assumed a correlation area of 1 km^2.

Our errors in B_a using a GPS arise from few upper-elevation measurements, and the lack of glacier-wide elevation measurements may bias $dh(z)$ (Figs. 2.5 and 2.7). I estimate interpolation error of ±0.57 m, based on the residuals between a two-piece linear

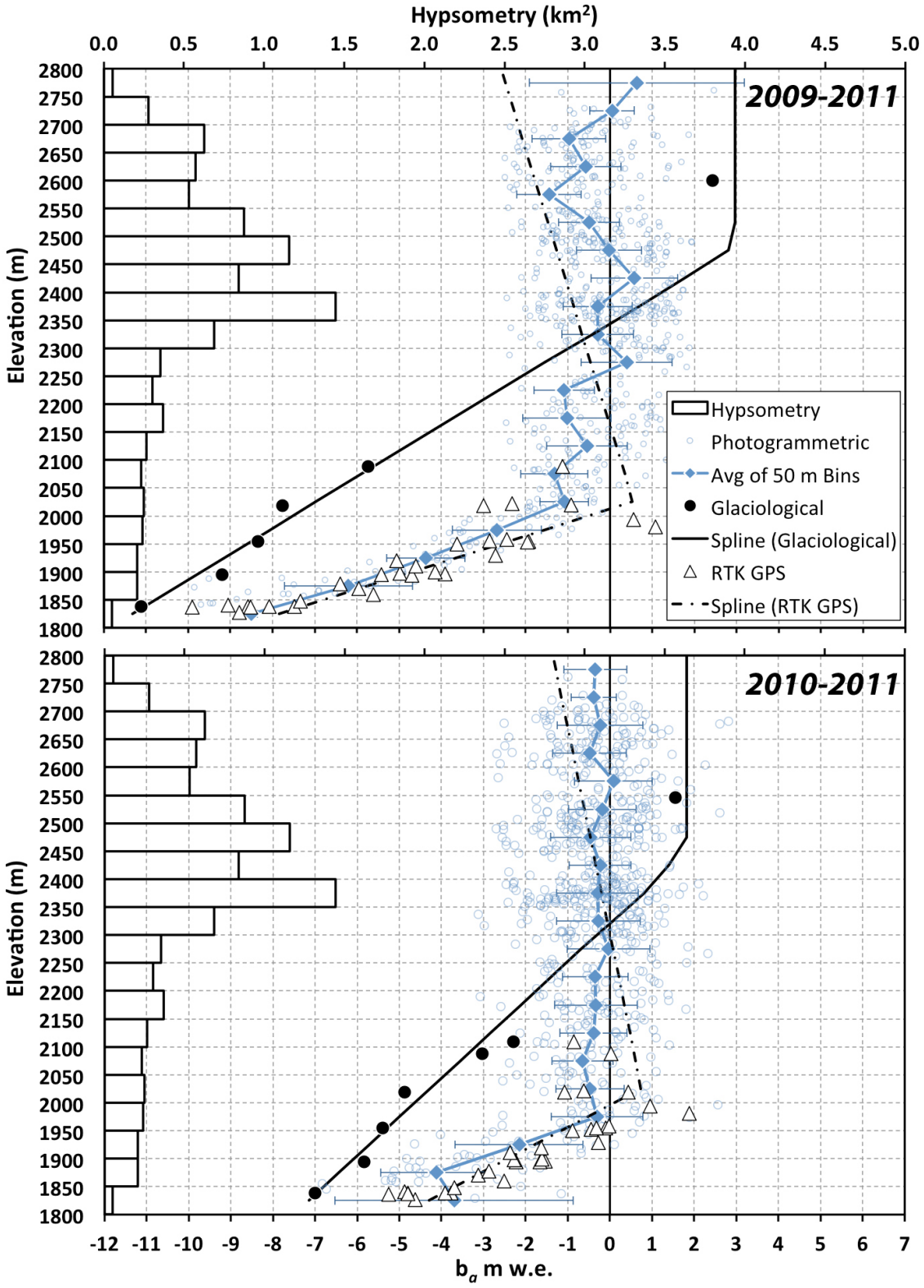

Figure 2.7 Same as Figure 2.5, but for two multi-year periods: 2009 – 2011 and 2010 - 2011.

spline and observations for 2011; a shorter monitoring period (August-September 2009) where I could make measurements in both the ablation and accumulation zones yielded a smaller interpolation error (±0.17 m). However, I cannot reliably determine $dh(z)$ for the GPS method given the lack of suitable accumulation zone measurements. Further investigation should be made using the GPS method with measurements well distributed across the entirety of a glacier's surface, and with the rover antenna on a stadia rod to maximize measurement precision.

To convert my geodetic measurements of dh to B_a m w.e. I used a bulk density of 810 ± 90 kg m^{-3}, which is similar to the density of 850 ± 60 kg m^{-3} recommended by Huss (2013). My estimated error due to assumed density (±0.05 to ±0.15 m w.e.) is lower than other error sources used in my geodetic estimates of mass change. Density errors annually vary due to the changes in extent of ablation and accumulation zones, and the magnitude of dh. However, I find error from density assumptions to be minimal on an annual basis.

I do not attempt to quantify errors due to advection of topography, but recognize that this process may inflate geodetic errors of B_a, especially in cases when the photogrammetric method does not sample the entire glacier surface. I observed topographic advection on a number of occasions as I navigated back to a point for re-measurement via GPS and found a crevasse where a relatively level surface existed previously. This same advection of surface features also likely plays a role in the apparent 'blunders' in my photogrammetric methodology, particularly over the minor, mid-glacier icefall.

2.6.2. Bias

All three methods used in this study differ in their sources of systematic bias. My glaciological measurements may include a positive bias from the omission of internal and basal mass balance. The photogrammetric measurements include a negative bias introduced by the manual operator and my temperature index model. In contrast, the GPS data do not include these biases.

The glaciological method suffers from potential biases associated with probing the previous summer surface, and no measurement of internal and basal mass-balance. My profiles of cumulative mass balance are more positive than cumulative values for my upper-most pit alone (Fig. 2.7), indicating a potential positive bias of the probing measurements. I use the average difference (0.07 m w.e.) between B_a derived from all points and only from pits as an approximation of this potential bias.

Sinking (self drilling) of ablation stakes may produce a negative bias in the glaciological method (Riedel et al., 2010). I tested this possibility by measuring ablation at adjacent stakes, one with an insulated cap at the base of the stake and one without. No differences were noted, and I thus assume that self-drilling did not occur.

Glaciological measurements do not capture internal and basal mass balance. These mass changes are glacier dependent, with internal and basal accumulation playing a more significant role in cold, continental climates (e.g., Storglaciaren, Sweden; Zemp et al., 2010), whereas internal and basal ablation dominates in warm, maritime climates (e.g., Franz Josef Glacier, New Zealand; Alexander et al., 2011). Castle Creek Glacier is a temperate, continental glacier and does not experience a high geothermal flux. Estimates of internal ablation for temperate glaciers vary dramatically from 1 cm w.e. a^{-1}

Table 2.3 Varying photogrammetric B_a results when using different melt factors in my temperature index model correcting for dates of photography. Percentages in parentheses indicate differences from results using Place Glacier melt factors.

Balance Year	Place* (m w.e.)	Castle Creek† (m w.e.)	Combined‡ (m w.e.)
2009	-0.15 ± 0.36	-0.19 ± 0.36 (-31%)	-0.11 ± 0.36 (+18%)
2010	no data	no data	no data
2011	no data	no data	no data
2009 - 2011	-0.59 ± 0.33	-0.58 ± 0.33 (+2%)	-0.60 ± 0.33 (-1%)
2010 - 2011	-0.44 ± 0.26	-0.36 ± 0.26 (+17%)	-0.47 ± 0.26 (-10%)

*Place Glacier melt factors: $k_s = 2.76$, $k_i = 4.67$ (mm w.e. $°C^{-1}$ d^{-1})

†Castle Creek Glacier melt factors: $k_s = 3.45$, $k_i = 4.33$

‡Place Glacier snow, Castle Creek Glacier ice melt factors: $k_s = 2.76$, $k_i = 4.33$

(e.g., Thibert et al., 2008) to 2.5 m w.e. a^{-1} at lower elevations (Alexander et al., 2011). I conservatively estimate internal ablation and accumulation to respectively be 10% and 4% of B_a (Zemp et al., 2010; Alexander et al., 2011). Combining these values with my probing bias, I estimate positive biases of 0.08, 0.09, and 0.10 m w.e. for the years 2009, 2010 and 2011 respectively, and 0.27 and 0.19 m w.e. for periods 2009-2011 and 2010-2011 respectively.

I corrected for stereo model bias in my photogrammetric measurements of B_a, but neglect densification and sub-glacial erosion, processes that I assume to be negligible in my study. To assess bias in the temperature index model I differenced modeled from observed ablation at array points for August 2008, 2009, and 2010. The mean of the residuals for 64 observations in the ablation zone is 0.02 m w.e., whereas it is -0.24 m w.e. for seven observations in the accumulation zone, suggesting a possible negative bias. However, this potential bias is perhaps related to error in my probing measurements at the seven accumulation-zone locations, and the limited number of observations. When comparing observed and modeled ablation measurements, I found melt factors derived

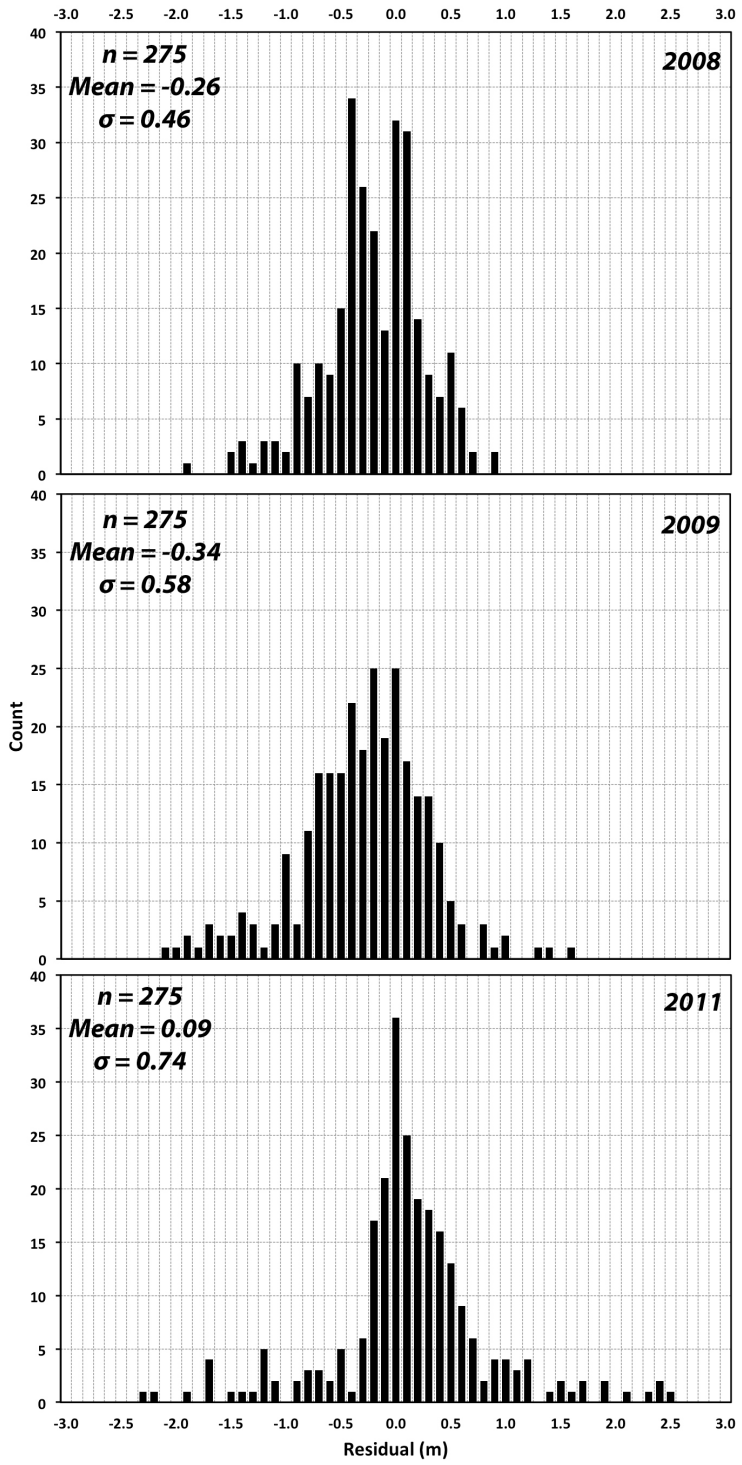

Figure 2.8 Frequency distributions of repeat-measurement residuals of 275 check points for stereo models from 2008, 2009, and 2011 aerial photography used to constrain potential error and bias of the analyst in manual photogrammetry. Each distribution displays surface-elevation residuals, defined as the difference in surface elevation of the same horizontal coordinates from the same stereo model and by the same operator, but from initial measurements and a repeat measurement at a later date.

from mass-balance measurements (Shea et al., 2009) yielded better agreement when using Place Glacier melt factors (-0.01 ± 0.20 m w.e.) than those from Peyto Glacier (+0.23 ± 0.28 m w.e.). I am hesitant to rely on Castle Creek Glacier melt factors given my short period of observation and few measurements for snow surfaces (n = 7). The use of melt factors derived from either Place of Peyto Glacier (Shea et al., 2009) does not substantially affect my estimated photogrammetric mass change (Table 2.3).

After correcting for stereo model bias, manual digitization can still introduce significant bias in photogrammetric measurements of *dh* (McGlone et al., 2004). My repeated measurements from the same stereo models of 275 check points assess this bias (Fig. 2.8), and yield a potential bias of -0.26 ± 0.46, -0.34 ± 0.58, and 0.09 ± 0.74 m for stereo models from 2008, 2009, and 2011 respectively. The mean of all 825 points gives a bias of -0.15 m. These results indicate a potential manual-operator bias, but one that is inconclusive in terms of both sign and magnitude. Additionally, measurement uncertainty varies according to glacier surface characteristics. Repeat measurements of surface elevation from 2009 models yielded residuals of 0.01 ± 0.44, 0.16 ± 0.66, and -0.15 ± 1.44 m ice eq. for ice, firn and snow respectively. This error, however, did decrease with repeated measurements, revealing the importance of operator experience (Fig. 2.4). I found that GPS and photogrammetric point measurements of *dh* accord in the ablation zone (Figs. 2.5A and 2.7).

I am unaware of other studies assessing the potential biases of GPS B_a measurements, and I do not attempt to quantify GPS bias, which would require a complete understanding of a glacier's spatially varying vertical velocity.

The two geodetic methods give results that are comparable to, or significantly more negative than those of the glaciological method. These results indicate negative biases inherent in the geodetic method or positive biases in the glaciological method, similar to findings at South Cascade Glacier (Krimmel, 1999). Other studies detect no systematic difference between the two methodologies (Cogley, 2009; Fischer, 2011).

2.6.3. Estimation of vertical velocity

My estimates of ablation, *dh*, and estimated vertical velocity for the ablation zone vary for the years 2008, 2009, and 2010 (Fig. 2.9). My method of estimating vertical velocity (Eqn (2.7)) yields values that average 0.30 m ice eq. more emergence than estimates from Eqn (2.4). GPS measurements at seven points in the accumulation zone in 2009 produce a submergence estimate of -0.38 ± 0.15 m ice eq.

I do not quantify errors in my estimate of vertical velocity. Using my approach, this error term will be dominated by advection of surface topography, but I lack a detailed estimate of the glacier's surface roughness. Advection of an irregular surface (0.5-2 m roughness) will greatly exceed my estimated precision in measuring height change from ablation stakes or with a GPS (±0.10 m ice eq.). I suspect that some of the variability in vertical velocity (Fig. 2.9) may arise from advection of topography.

2.7. Discussion and recommendations for future mass-balance monitoring

Limitations and advantages are inherent in each method to assess glacier mass change. Surface mass balance estimated by the glaciological method should be continued for index glaciers and potentially expanded for under-represented mountainous regions.

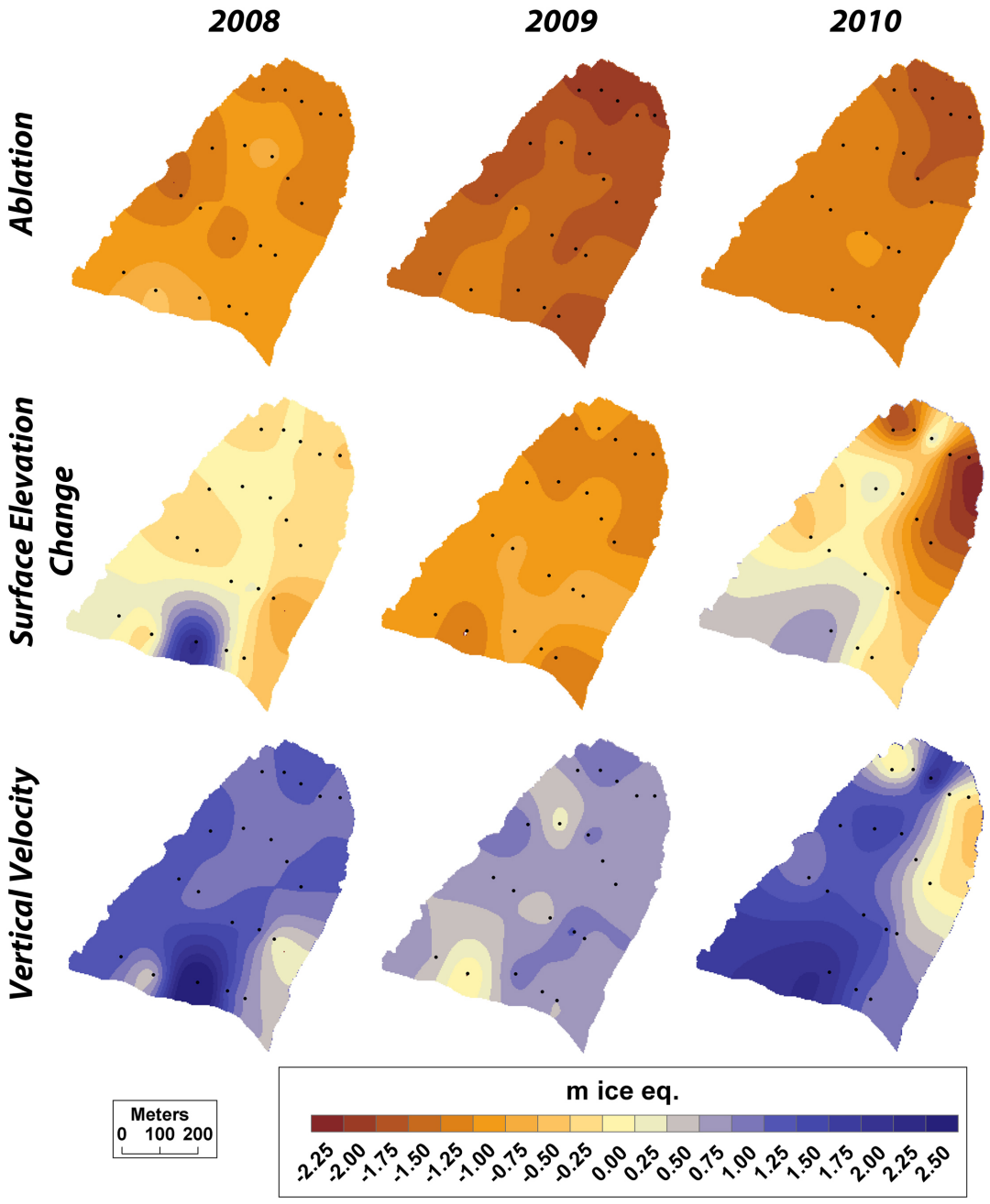

Figure 2.9 Spatial distribution of mass balance, thickness change, and vertical velocity from the 20-point ablation-zone array for the month of August in 2008, 2009, and 2010. All measurements in ice equivalent units. I derived mass balance from stake measurements, thickness change from RTK GPS, and vertical velocity as the difference of the two. Locations of stakes and GPS measurements are indicated by black dots.

A key benefit of the glaciological method is its ability to record $b(z)$, a prerequisite for modeling the response of a glacier to changes in climate (e.g., Radić and Hock, 2011). Unfortunately, the glaciological method also suffers from a number of logistical shortcomings, which include the time and energy intensive nature of the method, and its limitation to glaciers that are relatively small and safe for travel.

I recommend increased use of the photogrammetric method to monitor B_a. When GCPs already exist, fieldwork is not necessary, which can significantly reduce measurement time and cost. However, a lack of density measurements remains a source of error. Remote sensing geodetic methods afford the best possibility to monitor representative glaciers, including those that are large, complex and difficult to visit. Additionally, such methods enable the monitoring of more glaciers in a region, avoiding expensive and time intensive field studies.

Poor contrast, particularly for glaciers covered by fresh snow cover, limits the use of manual or automated feature extraction from aerial photography (e.g., Krimmel, 1999; Bamber and Rivera, 2007). Multispectral aerial photography or high-resolution, multi-spectral satellite imagery improves contrast in the accumulation zone of glaciers, however. The inclusion of the near infrared band in my 2011 stereo models, for example, enabled me to measure elevation for 74% of the glacier's surface that was covered by fresh snow.

I advocate the adoption of my GPS technique to measure B_a. Previous studies concluded that geodetic measurements alone cannot be used to measure B_a in the absence of a knowledge of dynamics (e.g., Hagen et al., 2005), but I find that a well-distributed subset of point measurements can adequately mitigate the confounding role of vertical

velocity to yield reliable estimates of B_a. In the case of Castle Creek Glacier, I find a sample density of 4 km^{-2} can be used to derive B_a using geodetic-grade GPS receivers (Fig. 2.6). If completed for a well-distributed subset of points across the glacier surface, the GPS method may circumvent some of the limitations inherent in the other two approaches, but more studies are required to quantify errors and bias inherent in the GPS approach.

Use of the *in situ* GPS method is restricted to those glaciers that are accessible, and safe for travel. Additionally, measurements yield *dh,* which is modulated by vertical velocity, making the GPS method ill-suited for determination of b_a and $b(z)$ (c.f. Figs. 2.5 and 2.7). GPS is advantageous on larger glaciers where the glaciological method is impractical due to necessary commitments of time and energy. Use of the GPS method at the end of the accumulation season, when glacier surfaces are covered with snow, may enable travel and measurement on surfaces inaccessible at the end of the balance year. I recommend future efforts to refine the GPS method be undertaken at an established field station with a source of power adequate for the high-powered base station radio (35W).

Combining at-a-point glaciological and GPS measurements provide one method to assess the spatial and temporal changes of vertical velocity for a glacier. My methodology to estimate vertical velocity (Eqn (2.7)) compares well with that of the geometric relation at the surface (Eqn (2.4)). However, a major shortcoming is that it is field-intensive, whereas it is possible to employ the kinematic boundary condition remotely (e.g., Gudmundsson and Bauder, 1999). Furthermore, the use of an Eulerian frame of reference in this method imparts a potential error due to advection of topography, an error that is likely to be on the order of 0.5 m, but may be in excess of 5

m in areas of complex surface topography. Changes in ice flux have been found to be significant in determining recent thinning (Berthier and Vincent, 2012), and combining GPS and glaciological measurements allows insight into the fine-scale structure of seasonal ice dynamics. Additionally, my *in situ* methodology enables the estimation of submergence in the accumulation zone. Remote sensing studies, which derive submergence from measurements of horizontal motion and elevation change (Eqn (2.4)), often fail in the accumulation zone due to a lack of surface features to track to determine surface velocity. However, a study of the potential error imparted by advection of topography is required.

My future efforts at Castle Creek Glacier will include continued monitoring of annual length change (Beedle et al., 2009), and glaciological measurements of annual mass balance. Additionally, I plan to acquire aerial photographs of Castle Creek Glacier annually for geodetic measurements of annual and cumulative mass balance.

There is a need to continue long-term mass-balance measurements, resume interrupted series, expand to important regions and more representative glaciers, and improve error analysis (Fountain et al., 1999; Zemp et al., 2009). Geodetic methods provide a valuable measure of B_a that is complementary to those of the glaciological method. Photogrammetric and GPS methods provide means to improve understanding of glacier change, and to help understand and predict the fate of mountain glaciers.

3. Annual Push Moraines as Climate Proxy

Publication details:

This chapter has been peer reviewed and is published in Geophysical Research Letters. Please see Appendix A: Authorship Statements for details of the contributions of each author.

Beedle, M. J., Menounos, B., Luckman, B. H. and Wheate, R. 2009. Annual push moraines as climate proxy. *Geophysical Research Letters,* 36, L20501 (doi:10.1029/2009GL039533)

3.1. Abstract

I reconstruct the terminus position of a mountain glacier in British Columbia, Canada from annual push moraines formed between 1959 and 2007. My reconstruction represents the longest, annually-resolved record of length change for a North American glacier. Comparison of annual recession with climate records indicates that glacier recession is controlled by air temperatures during the ablation season and accumulation season precipitation during the previous decade. Analysis among records of glacier frontal variation and mass balance in western North America similarly reveals an immediate terminus reaction to summer and net mass balance and a delayed reaction to winter and net balance. Other mountain ranges may contain long series of push moraines

that could be exploited as climate proxies, and to improve understanding of glacier response to climate.

3.2. Introduction

Mountain glaciers provide fresh water to millions of people, and contribute to global sea level rise (Barnett et al., 2005; Meier et al., 2007). Records of glacier terminus fluctuations and mass balance provide insight into how climate affects this important freshwater source. Meier et al. (2007) estimate there are 300,000 to 400,000 mountain glaciers and small ice caps on Earth, but length change and mass balance records exist for only 1,800 and 230 glaciers, respectively. Only 39 of these glaciers have records that exceed 30 years in length (Zemp and van Woerden, 2008), and there is a strong European bias in these records.

I use push moraines to reconstruct the longest, annually-resolved record of terminus position for a North American glacier. Glaciers form annual push moraines during the accumulation season when forward movement of the glacier snout exceeds ablation, resulting in a seasonal advance (Bennett, 2001). Formation of a push moraine at the glacier margin requires a deformable till sheet. Preservation of annual moraines requires ablation season recession to be greater than advance of the terminus during the following accumulation season. To my knowledge, all studies of annual push moraines are for maritime glaciers with high mass-balance gradients in either Iceland (Sharp, 1984; Boulton, 1986, Krüger, 1995; and Bradwell, 2004) or Norway (Andersen and Sollid, 1971; and Worsley, 1974).

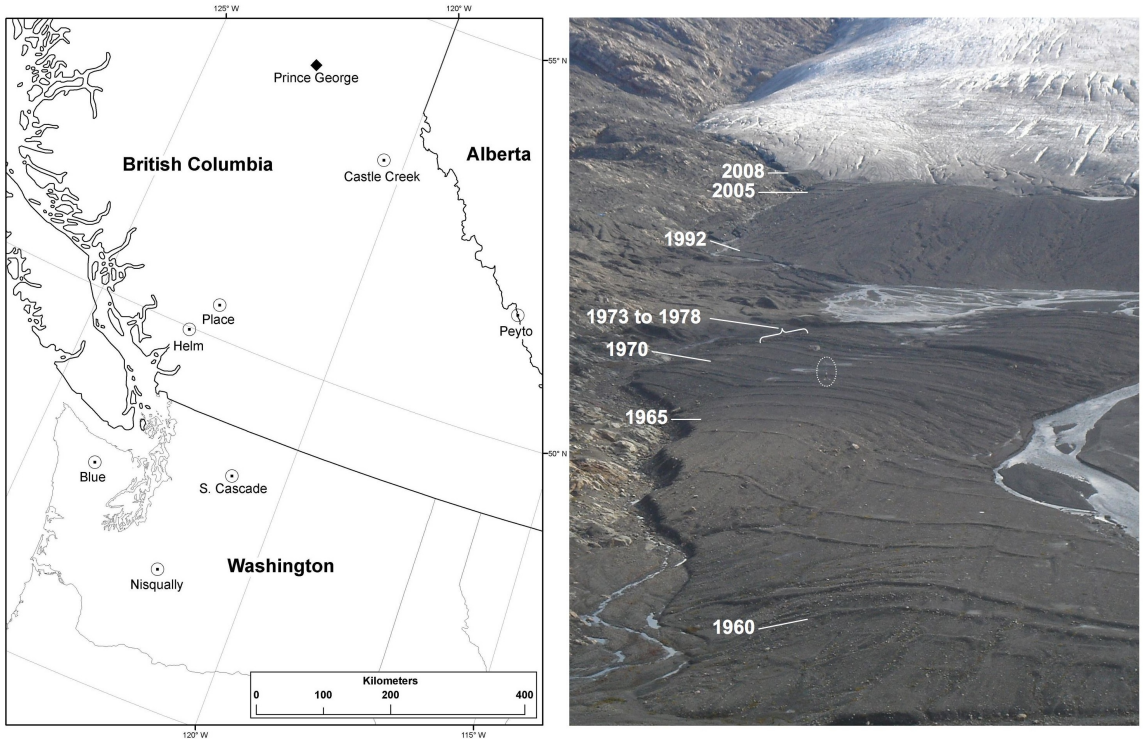

Figure 3.1 A) Location of glaciers and climate stations referenced in this paper; B) Oblique photo of a portion of the Castle Creek Glacier forefield taken 11 September 2008. Dates refer to the year of moraine formation. The white circle encloses a 6 m high weather station. Some moraines used in my study are not visible in this photo.

3.3. Study area and methods

I reconstructed the frontal position of Castle Creek Glacier (53° 2′ N., 120° 24′ W., unofficial name), British Columbia (BC), Canada from a continuous series of push moraines that front the glacier (Fig. 3.1). The glacier has an area of 9.4 km^2, a length of 5.85 km, and an elevation range of 2,827 to 1,810 m.

To determine the age of the moraines, I mapped glacier terminus position for 10 dates between 1946 and 2005 from orthorectified aerial photographs (Table 3.1). I photogrammetrically scanned aerial photograph negatives from the Canadian and BC governments with a ground sampling resolution of ≤ 1.0 m. To orthorectify these images, I used common ground control points and the 25 m BC Terrain Resource

Table 3.1 Descriptive data for the 10 aerial photos used in this study. 'A' denotes federal photography, accessed from the National Air Photo Library, Natural Resources Canada, Ottawa, Ontario. 'BC' denotes provincial photography, Crown Registry and Geographic Base, Victoria, British Columbia.

Date	Roll ID	Nominal scale
1946-09-10	BC321	1:31,680
1952-09-25	A13538	1:60,000
1967-08-15	BC7019	1:15,840
1971-07-15	A21587	1:80,000
1973-08-11	BC7523	1:15,000
1977-07-24	A24743	1:60,000
1984-07-31	BC84073	1:60,000
1991-08-22	BCB91102	1:15,000
1996-09-11	BCB96106	1:40,000
2005-08-25	BCC05111	1:20,000

Information Management Program digital elevation model (DEM). Root mean squared error of these horizontal control points was ≤ 1.6 m and typically below 1.0 m. I surveyed push moraines that formed after my latest aerial photographs (2005), and terminus position at the end of the ablation season in 2007 and 2008 with a geodetic-grade global positioning system.

Annual push moraine position indicates a prior maximum glacier extent achieved at the end of the accumulation season, while glacier terminus position is mapped from imagery acquired at the end of the ablation season. Thus, I dated the push moraines immediately down-valley of the known terminus position as being formed at the end of the previous accumulation season. The number of intervening moraines coincides with the years between consecutive images, confirming the annual nature of the moraines. I represent changes in glacier length as the total area between moraines or mapped terminus position divided by the curvilinear width. This method integrates recession across the entire glacier terminus and accounts for retreat along an irregular glacier margin.

To examine the climatic controls on mass changes and related frontal variation, I compared glacier length change records derived from annual push moraines with homogenized climate station records of air temperature and precipitation (Vincent, 1998; Mekis and Hogg, 1999) from the Prince George, BC climate station, ~180 km to the northwest (Fig. 3.1). For my study, I define ablation season as April - September and accumulation season as October - March. I compared un-lagged and lagged total accumulation season precipitation to assess the role of total accumulation during the following ablation season and a delayed terminus reaction to a precipitation signal integrated over the glacier surface.

To evaluate the representativeness of length change records derived from annual push moraines, I compared the record from Castle Creek Glacier to annual and seasonal mass balance series and glacier length change records from western North America (Tables 3.2 and 3.3). I used cross-correlation analysis to investigate the lagged relation between seasonal (b_w and b_s) and annual (b_a) mass balance and frontal variation. McClung and Armstrong (1993), Laumann and Nesje (2009), and Winkler et al. (2009) compared b_a with frontal variation, but I am unaware of previous analysis that considers the relation between frontal behavior and seasonal mass balance.

The bed slope near the glacier terminus can affect frontal reaction of a glacier as the position of the terminus depends on ice velocity and the product of bed slope and ablation near the snout (Nye, 1965; Boulton, 1986). To investigate the potential role that bed gradient plays as a control of annual glacier length change, I compared the frontal recession for a given year to the average bed slope obtained between two consecutive push moraines. I used two DEMs to assess slope: the 25 m DEM used for image